AIP/123-QED

Complex plume stoichiometry during pulsed laser deposition of $SrVO_3$ at low oxygen pressures

Jun Wang,[1] Guus Rijnders,[1] and Gertjan Koster[1, a)]

Faculty of Science and Technology and MESA+ Institute for Nanotechnology, University of Twente,7500 AE Enschede, The Netherlands

(Dated: 20 October 2018)

To control the pulsed laser deposition synthesis, knowledge on the relation between the plasma plume and the grown thin film is required. We show that the oxidation of species in the plasma plume still affects the $SrVO_3$ growth at low oxygen partial pressures. Optical emission spectroscopy measurement for the plasma plume at different growth conditions were correlated to the film properties determined by Atomic force microscopy, X-ray diffraction and transport. At reducing oxygen pressures, the background argon pressure can affect the oxidation in the plasma plume, which in turn controls the growth kinetics, stoichiometry and electrical properties of the films.

a)Electronic mail: g.koster@utwente.nl

Transition metal oxides with the perovskite structure have received a lot of interest in recent years due to their broad range of properties, such as metal-to-insulator transitions, ferroelectricity and superconductivity. These properties open the way for novel applications, for example transistors, switches and sensors.[1,2,3].

The materials properties of thin film are related to surface morphology and crystal quality, which in turn are mostly determined by surface kinetics. Pulsed laser deposition (PLD) is a widely used thin film deposition technique. One of most cited reasons for its popularity is that it enables the deposition of a broad range of materials which can be stoichiometrically transferred from target to substrate. However, in reality the exact distribution and nature of species being transferred and their influence on surface kinetics and growing film are still little known. The most generally adopted model is that the kinetic energy of the arriving species is the key parameter to determine the type of the growth mechanism[4,5]. The relation between the ambient gas pressure and kinetic propagation characteristics of the expanding plasma plume is well-known: the plasma propagation behaviour evolves from thermalized to drag with increasing background gas pressure[6,7]. The model suggests that the increased kinetic energy of the species at lower background gas pressures improves surface diffusion which is favourable to the crystallinity and the smoothness of the films[8,9]. More recent work has shown that oxidation of the arriving species also plays a role in controlling the smoothness and stoichiometry of the grown films[10]. In the pressure range where the kinetic transition occurs, the authors investigated the $SrTiO_3$ growth at varying oxygen pressure in the range from 0.01 mbar to 0.1 mbar. Oppositely to kinetic model, this work showed that stoichiometric and smooth films were obtained at higher oxygen pressures. The Titanium atoms are oxidized to TiO_2 in the plasma plume at increased oxygen pressure and Ti^{4+} is the most steady oxidation state for Titanium. Based on previous studies of plasma chemistry and thin film growth, which were conducted at relatively high absolute oxygen pressure, the question addressed in this study is whether oxidation of species plays any role at much lower oxygen pressure. $SrVO_3$ is a good material system to study the influence of the growth parameters on oxide thin film characteristics such as stoichiometry and surface morphology at a low oxygen pressure range. $SrVO_3$ can only be grown in very low oxygen (partial) pressure since over-oxidized V^{5+} hampers perovskite $SrVO_3$ to be formed. V^{4+} in $SrVO_3$ has tendency to dismutate: V^{4+} can be over-oxidized to V^{5+} at high oxygen pressure and oxygen vacancies can also be formed under reducing conditions[11,12]. $SrVO_3$ recently gains

a lot of attention due to its high electrical conductivity[12,13]. Although $SrRuO_3$ has been widely used as an electrode layer in oxide thin film heterostructure and this material fulfils most requirements in many applications[14,15,16,17,18], a much lower resistance is still desired for high frequency applications to reduce conduct losses. $SrVO_3$ has also been studied recently as a transparent conductor[19] and has been widely studied in theoretical modes as a correlated system[20,21]. To investigate whether the nature of species has an influence on the thin film growth at low oxygen pressure, we grew the $SrVO_3$ films at varying total pressures or varying oxygen partial pressures.

For a typical used target-to-substrate (T-S) distance of 50 mm, the change in kinetic propagation behaviour of the species occurs above 0.01 mbar[7,10]. At low oxygen pressure, an argon pressure was introduced to control the propagation of the expanding plasma plume. All of thin films were grown using a PLD system equipped with reflection high energy electron diffraction (RHEED). During growth all films were monitored using RHEED to study the growth kinetics and in-plane crystal structure. A thermal and chemical treatment was applied to achieve the single TiO_2 terminated $SrTiO_3$ (100) (STO) substrates[22]. A KrF excimer laser ($\lambda = 248nm$) at fluency of 2 J/cm^2 and 1 Hz repetition rate was used. Temperature was kept at 600 $^{\circ}C$. Four samples in the first set were grown in the argon pressures of 0.01 mbar, 0.02 mbar, 0.025 mbar and 0.04 mbar with the same oxygen partial pressure of 1×10^{-5} mbar. The second set of samples were deposited in the 0.025 mbar argon pressure with different oxygen partial pressures of 1×10^{-6} mbar, 5×10^{-6} mbar and 1×10^{-5} mbar. With a constant background total pressure, and only varying the oxygen partial pressure, we should be able to separate the effects of oxidation and plasma species kinetics. The thickness of the films is kept at about 30 nm in this study.

Atomic force microscopy (AFM) (Bruker) in tapping mode was used for characterizing the topography of the obtained films, which indicates the type of the growth mechanism. X-ray diffraction (XRD) (Xpert panalytical MRD) was used to characterize crystal structure of the thin films. The out-of-plane lattice constant can be derived by performing $2\theta/\omega$ symmetrical scans around the (002) Bragg reflection of $SrTiO_3$ substrate to indicate the stoichiometry of grown films. Transport properties were measured in the van der Pauw geometry using a Quantum Design Physical Properties Measurement System (QD PPMS) in the 2 K - 300 K temperature range.

To correlate the changes in nature of species being transferred with crystallinity and

smoothness of the films, optical emission spectroscopy (OES) measurements for the $SrVO_3$ plume were performed at the thin film growth conditions. An intensified charge coupled device (ICCD) camera (Andor New iStar) connected with a spectrograph (Andor's Shamarock) was used to collect the data. The targets of SrO, V_2O_5 and V_2O_3 were also inspected to get information about the individual element in $SrVO_3$. The wavelength scale was calibrated using reference database[23]. We focus on the wavelength in the range from 470 nm to 530 nm for neutral Strontium and in the range from 600 nm to 640 nm for oxidized Vanadium. A bandpass of 257 nm and a spectral resolution of 1.5 nm can be obtained by using a 1024×1024 pixel array and a 300 lines/mm grating. Each spectrum was taken at different delay time τ after the target ablated.

Figure 1 shows AFM images and the corresponding cross-section profiles of the samples grown at argon pressures ranging from 0.01 mbar to 0.04 mbar with the oxygen partial pressure of 1×10^{-5} mbar. The insets correspond to the RHEED diffraction patterns in the [01] direction after growth. The films grown at pressures below 0.025 mbar have an island morphology and the step-terrace structure of the substrate is barely visible (see Figure 1 (a) and (b)). The corresponding RHEED patterns are so-called streaky patterns which are indicative of a still relatively two dimensional flat and crystalline surface. The peak-to-peak height difference is about 0.5 nm for these films as seen in the cross section profiles. On the other hand, the step-terrace structure is more clearly observed for the film grown at 0.025 mbar (shown in Figure 1 (c)). Presumably step-flow-like growth has occurred at the latter condition. The RHEED specular intensity versus time for this film is shown in Figure S1, which additionally supports step-flow-like growth. The cross-section profile shows that the peak-to-peak height difference is about 1 nm. This value is higher than that in the previous two samples, because in addition to the flat terraces, the image also reveals trenches at the edge of each terrace. Their origin is not fully understood, however, similar trenches have been seen in $SrRuO_3$ thin films, which are related to the surface termination[14]. Finally, Figure 1 (d) shows that 3D islands are formed for the film deposited at 0.04 mbar, with heights of more than 4 nm. It is also confirmed by RHEED showing a 3D transmission pattern.

Figure 2 shows AFM images of the films grown at varying oxygen partial pressures of 1×10^{-6} mbar, 5×10^{-6} mbar and 1×10^{-5} mbar with the constant argon pressure of 0.025 mbar. AFM images show a layer-by-layer growth mode for the film grown at the 1×10^{-6}

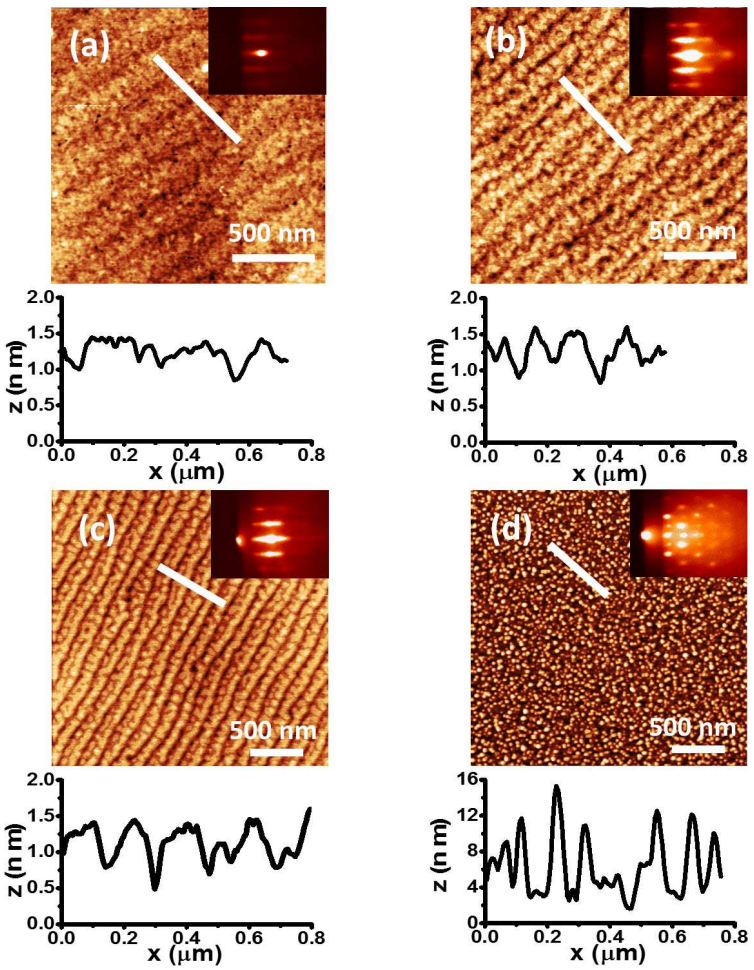

FIG. 1. AFM images of $SrVO_3$ thin film grown at the same oxygen partial pressure of 1×10^{-5} *mbar* and varying argon background pressures of (a) 0.01 mbar, (b) 0.02 mbar, (c) 0.025 mbar and (d) 0.04 mbar. Each inset shows the RHEED pattern and a cross-section at each white line is shown below the AFM image.

mbar and 5×10^{-6} mbar. At 1×10^{-6} mbar, Figure 2 (a) shows that the initial terrace morphology of the substrate surface is still visible. However the morphology consists of very small islands on the terraces. The islands are too small to cover the terrace edge in the substrate. The cross-section profile shows that the peak-to-peak difference is about 1 nm. The inset RHEED pattern shows a streaky pattern. The arriving species are more likely to be nucleated in Figure 2 (b). The size of islands in Figure 2 (b) is larger than that of islands in Figure 2 (a). The large islands are easily to cover the terrace edges, causing substrate imprint is absent. The peak-to-peak difference is 1 nm as shown in the cross-section profile. The inset RHEED pattern also shows a so-called streaky pattern. Figure 2 (c), the same

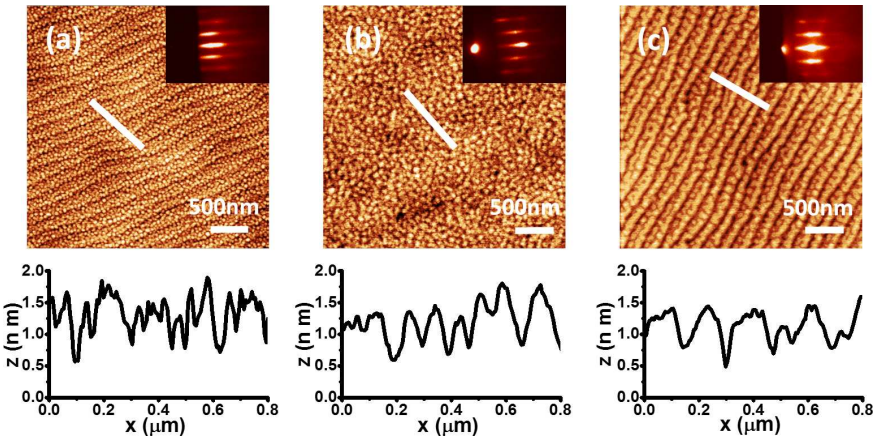

FIG. 2. AFM images of $SrVO_3$ thin film grown at oxygen partial pressures of (a) 1×10^{-6} mbar, (b) 5×10^{-6} mbar and (c) 1×10^{-5} mbar with the same argon pressure of 0.025 mbar. Each inset shows the RHEED pattern and a cross-section at each white line is shown below the AFM image.

image as shown in Figure 1 (c), shows a clear step-terrace structure for the film grown at 1×10^{-5} mbar. This is an evidence for a step-flow-like growth mode. The kikuchi lines are visible in the corresponding RHEED pattern, which indicates a highly-ordered surface.

Figure 3(a) shows XRD 00l scans around the (002) Bragg reflection of $SrTiO_3$ for the films grown at varying argon pressures. AFM images of these samples were shown in Figure 1. The (002) film peaks of $SrVO_3$ are indicated by black arrows. The measurements are fitted using the Stepanov model for quantitative analysis[24] and the corresponding out-of-plane lattice parameters are shown in Table I. The reciprocal mapping around $SrTiO_3$ (103) (See Figure S2) showed that the $SrVO_3$ film is fully in-plane strained by the $SrTiO_3$ substrate. The equi-biaxial strain in the film plane due to lattice mismatch between STO (3.905 $\mathring{A}$) and SVO (3.842 $\mathring{A}$) is 1.64%. Assuming the possion's ratio for SVO is 0.28[12], the expected out-of-plane lattice parameter for stoichiometric SVO film is 3.793 $\mathring{A}$. An increase of the film c-axis length corresponds to an increase unit cell volume which is caused by cation nonstoichiometry or point defects in the lattice[10,12]. As the out-of-plane lattice parameter decreases with the increasing argon pressure, the film grown at higher pressure is closer to stoichiometry. The Laue fringes around the films peaks originating from the coherence between individual layers in the film are observed for the film grown at 0.01 mbar, 0.02 mbar and 0.025 mbar, which also indicate a high degree of crystallinity. The thickness d of the grown film, listed in Table I, can also be derived from the spacing of the Laue fringes.

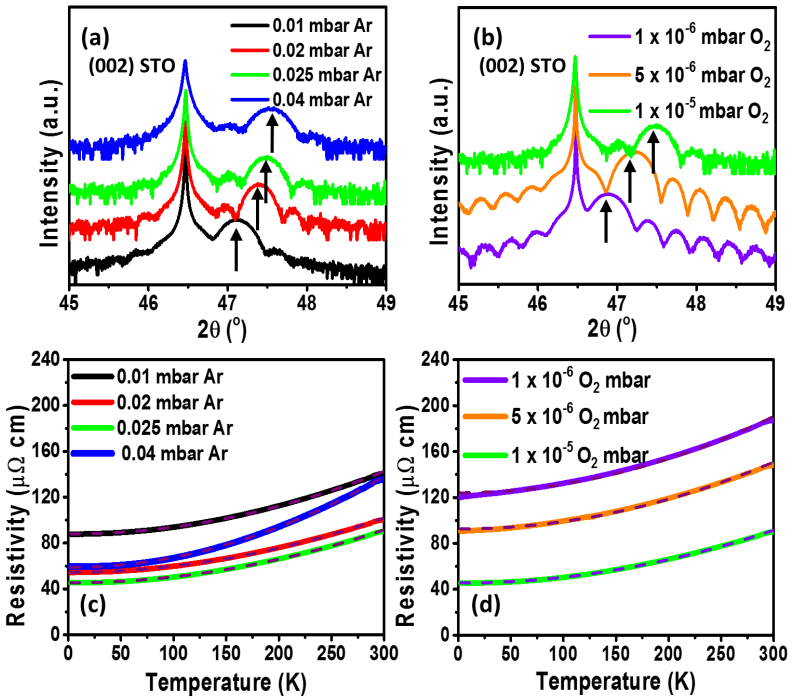

FIG. 3. XRD 00l scans around the (002) Bragg reflection of the $SrTiO_3$ for $SrVO_3$ thin film grown at (a) oxygen partial pressure of 1×10^{-5} mbar with varying argon pressures and (b) at argon pressure of 0.025 mbar with varying oxygen partial pressures. $SrVO_3$ film peaks are indicated by black arrows. Temperature dependent resistivity ρ for deposited $SrVO_3$ films grown at (c) varying argon pressures and (d) varying oxygen partial pressures. The purple dashed line shows the fitting of $\rho = \rho_0 + AT^2$ for each film.

Figure 3(b) shows the XRD 00l measurement of films grown at varying oxygen partial pressures. AFM images of these samples were shown in Figure 2. The out-of-plane lattice parameter and the thickness for the obtained films are shown in Table I using the same fitting algorithm. Again, an increased thin film c-axis length corresponds to an unit cell volume increased which results from point defects in the lattice. The XRD results suggest that the films grown in increasing oxygen partial pressure get closer to stoichiometric composition.

The temperature dependence of electrical resistivity was measured in the temperature range 2 K - 300 K, as shown in Figure 3 (c) and (d). All the samples show metallic behaviour: the resistivity decreases with decreasing temperature. Furthermore, the electrical resistivity as a function of temperature can be fitted by a $\rho = \rho_0 + AT^2$ relation (see purple dashed line),

TABLE I. Overview lattice parameters and thickness derived from the XRD scans for all samples.

P_{Ar}/P_{O_2}(mbar)	$C_{axis}(\mathring{A})$	d(nm)	No. of Pulses
$0.01/\ 1\times10^{-5}$	3.853 ± 0.001	31.0 ± 0.5	900
$0.02/\ 1\times10^{-5}$	3.833 ± 0.001	34.0 ± 0.2	950
$\mathbf{0.025/1\times10^{-5}}$	$\mathbf{3.826\pm0.001}$	$\mathbf{31.0\pm0.2}$	**900**
$0.04/\ 1\times10^{-5}$	3.819 ± 0.001	30.0 ± 0.5	900
$0.025/1\times10^{-6}$	3.870 ± 0.001	30.0 ± 0.2	900
$0.025/\ 5\times10^{-6}$	3.846 ± 0.001	30.0 ± 0.2	900

which is characteristic of a Fermi liquid behaviour. The fitting parameters are reported in Table S1. The lowest resistivity of 90 $\mu\Omega$ cm at room temperature is obtained for the film with the smoothest surface and the best stoichiometry, which is grown at 0.025 mbar argon pressure with the oxygen partial pressure of 1×10^{-5} mbar. In order to be able to convincingly exclude a contribution from the substrate, a bare STO substrate, which has been subjected to growth conditions of SVO, but without the actual deposition taking place, was measured by insulation tester (Fluke 1507). The sample remained highly insulating with resistivity of 146 MΩ cm. In addition, the same SVO thin film has been grown on $(LaAlO_3)_{0.3}(Sr_2AlTa_6)_{0.7}$ (LSAT) substrate, a material that should not be reducible under any condition, at the optimal growth conditions. The resistivity of the film at room temperature is about 70 $\mu\Omega$ cm (see Figure S3), which is even lower than the resistivity of the film grown on the STO substrate (90 $\mu\Omega$ cm). We think this data can also be a strong evidence to rule out the contribution from the STO substrate.

To investigate the composition of the plasma plume at varying growth conditions, optical emission spectroscopy (OES) measurement was performed on the expanding plume. Although these measurements only interpret the results qualitatively, they can still indicate the relative abundance of species in different growth conditions. To help identifying the spectrum for individual elements (Sr and V) in $SrVO_3$, plasma using different targets of V_2O_3, V_2O_5 and SrO were imaged. (shown in Figure S4). Their images indicate that the spectra at wavelength between 470 nm and 530 nm corresponds to neutral Strontium and the spectra at wavelength between 600 nm and 640 nm corresponds to oxidized Vanadium. The spectra of the oxidized Vanadium in the plasma plume of the $SrVO_3$ target are normal-

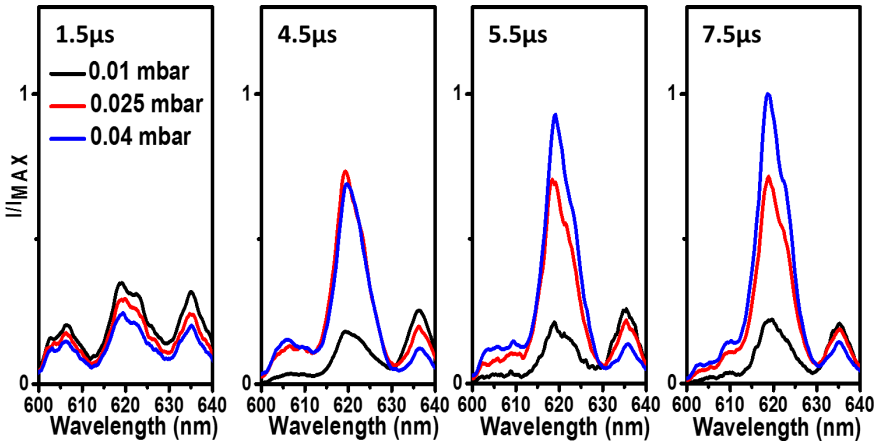

FIG. 4. The normalized spectra of the oxidized Vanadium in the plasma plume expanding of the $SrVO_3$ target.

ized by the maximum intensity of the plume expanding at 0.04 mbar, as shown in Figure 4. The $SrVO_3$ was ablated at varying total argon pressures of 0.01 mbar, 0.025 mbar and 0.04 mbar with the same oxygen partial pressure of 1×10^{-5} mbar. At $\tau = 1.5$ μs, the intensity of all peaks corresponding to oxidized Vanadium are very low, since the species in plume mostly are neutral just after the target to be ablated. For the measurement at 0.01 mbar, the intensity of the peak at wavelength of 620 nm is not changing over time (see black line). At 0.025 mbar and 0.04 mbar, presented in red and blue line, the intensity of peak at 620 nm is rapidly increasing after 4.5 μs. At $\tau = 5.5$ μs, the intensity of this peak for 0.04 mbar is higher than that of the peak for 0.025 mbar (see blue and red lines). The amount of the oxidized Vanadium in the plume increases with the total argon pressure increasing. This phenomenon is likely to be caused by the plume confinement due to scattering resulting from the argon pressure increasing. In addition, the plume expands more slowly at higher pressure, causing more species to be oxidized in the plasma plume.

The results from the structural investigation and plasma plume analysis show the relation between the thin film characteristics and the species in the plume. The XRD characterization shows that the c-axis of the grown films was dependent on the total argon pressure. It indicates that the stoichiometry of the thin films is the function of the total pressure increasing. The growth kinetics was indicated by surface morphology study using AFM. At 0.025 mbar argon pressure, presumably step-flow-like growth mode has occurred, implying the improved surface diffusivity at this condition. However, the 3D growth mode occurred

for the film grown at 0.04 mbar, indicating the limited mobility of particles at the substrate. The optimal room temperature resistivity of 90 $\mu\Omega\ cm$ was obtained for the film with the optimal crystalline structure and smooth surface morphology. The spectrum analysis indicates that the oxidized Vanadium in the plume was formed when the pressure increased to 0.025 mbar. An increased amount of oxidized species was observed at pressure of 0.04 mbar. These correlations strongly suggest that the oxidized species in plasma plume is a necessary requirement for stoichiometric growth thin film of $SrVO_3$. The amount of oxidized species determine the surface diffusivity at the substrate for the films grown with the optimal at argon pressure of 0.025 mbar. Apparently, an excess of oxidized species at an argon pressure of 0.04 mbar can cause the over-oxidation. We Speculate that mostly 4+ Vanadium is necessary to obtain the perovskite phase of $SrVO_3$. The kinetic model proposed in previous works assume that the diffusion activation energy increases with increasing pressure[8,9]. The model assumes that changing kinetic of arriving species affects the relaxation of the substrate. However, in this work surface smoothening and stoichiometric improvement are observed with the increasing background pressure up to 0.025 mbar. Therefore, we suggest that the enhanced surface diffusivity and improved stoichiometry are also dependent on oxidation of arriving species. A similar transition in the thin film stoichiometry and the surface morphology is observed for the films grown at varying oxygen partial pressures with the total pressure of 0.025 mbar. Since the kinetic energy is not changing, this supports the model of having the oxidation of arriving species to be an important parameter to affect the thin film growth. This suggests that oxidation of arriving species could determine the surface diffusion energies, but also could play a role in the competition between the formation of different phases, either through preferred nucleation or kinetically enhanced growth of island. These are topics for future investigations

To further substantiate this model, in supplementary information (see Figure S6 and S7), the structural property and surface morphology of the film grown at varying target-to-substrate (T-S) distances are investigated. The total argon pressure and the oxygen partial pressure was kept at 0.035 mbar (higher than the optimal pressure observed in previous experiments) and 1×10^{-5} mbar respectively. We observed the similar transition in the thin film stoichiometry and the surface morphology with increasing the T-S distance. An non-stoichiometry film was obtained at 28 mm. The step-flow-like growth occurred at the film grown at 42 mm, indicating the improved surface diffusivity by oxidized species. The

3D islands are observed for the film grown at 50 mm, implying an excess of the oxidized species. The plasma plume study suggests that the amount of oxidized species in the plume increase with the plume propagation from the target to the substrate at this pressure. This result also supports that surface diffusivity and film stoichiometry is dependent on oxidation of the arriving species at the substrate.

From the correlation between the thin films properties determined by AFM and XRD and plasma plume composition analysed by OES measurements. We conclude that the surface diffusivity, growth kinetic and the films stoichiometry are controlled by oxidation of arriving species. At reducing oxygen pressures, the spectrum of expanding plume indicates that the oxidation species in the plasma plume can be controlled by the total argon pressure, which in turn controls the quality of the thin films, including the electrical properties of $SrVO_3$.

SUPPLEMENTARY MATERIAL

See Supplementary material for the reciprocal mapping of $SrVO_3$ thin film, RHEED intensity of the thin grown in the optimal conditions, fitting parameters of resistivity as a function of temperature, optical emission spectroscopy spectra of plume of V_2O_3, V_2O_5 and SrO and AFM and XRD studies of the films grown at varying T-S distance.

This work was supported by Nederlandse Organisatie voor Wetenschappelijk Onderzoek through Grant No.13HTSM01.

REFERENCES

[1]M. Imada, A. Fujimori, and Y. Tokura, Rev. Mod. Phys. **70**, 1039 (1998).

[2]I. H. Inoue and M. J. Rozenberg, Advanced Functional Materials **18**, 2289 (2008).

[3]H. W. Jang, A. Kumar, S. Denev, M. D. Biegalski, P. Maksymovych, C. W. Bark, C. T. Nelson, C. M. Folkman, S. H. Baek, N. Balke, C. M. Brooks, D. A. Tenne, D. G. Schlom, L. Q. Chen, X. Q. Pan, S. V. Kalinin, V. Gopalan, and C. B. Eom, Phys. Rev. Lett. **104**, 197601 (2010).

[4]G. Koster, G. J. H. M. Rijnders, D. H. A. Blank, and H. Rogalla, Applied Physics Letters **74**, 3729 (1999).

[5]D. H. Blank, G. Koster, G. A. Rijnders, E. van Setten, P. Slycke, and H. Rogalla, Journal of Crystal Growth **211**, 98 (2000).

[6]S. Amoruso, A. Sambri, and X. Wang, Journal of Applied Physics **100**, 013302 (2006).

[7]D. B. Geohegan, Thin Solid Films **220**, 138 (1992).

[8]P. R. Willmott, R. Herger, C. M. Schlepütz, D. Martoccia, and B. D. Patterson, Phys. Rev. Lett. **96**, 176102 (2006).

[9]J. E. Boschker, E. Folven, s. F. Monsen, E. Wahlström, J. K. Grepstad, and T. Tybell, Crystal Growth & Design **12**, 562 (2012).

[10]R. Groenen, J. Smit, K. Orsel, A. Vailionis, B. Bastiaens, M. Huijben, K. Boller, G. Rijnders, and G. Koster, APL Materials **3**, 070701 (2015).

[11]S. Hui and A. Petric, Solid State Ionics **143**, 275 (2001).

[12]J. A. Moyer, C. Eaton, and R. Engel-Herbert, Advanced Materials **25**, 3578 (2013).

[13]Y. Lan, X. Chen, and M. He, Journal of Alloys and Compounds **354**, 95 (2003).

[14]G. Koster, L. Klein, W. Siemons, G. Rijnders, J. S. Dodge, C.-B. Eom, D. H. A. Blank, and M. R. Beasley, Rev. Mod. Phys. **84**, 253 (2012).

[15]Y. Kozuka, Y. Hikita, C. Bell, and H. Y. Hwang, Applied Physics Letters **97**, 012107 (2010).

[16]A. Vailionis, W. Siemons, and G. Koster, Applied Physics Letters **93**, 051909 (2008).

[17]M. Hiratani, C. Okazaki, K. Imagawa, and K. Takagi, Japanese Journal of Applied Physics **35**, 6212 (1996).

[18]G. Herranz, V. Laukhin, F. Sánchez, P. Levy, C. Ferrater, M. V. García-Cuenca, M. Varela, and J. Fontcuberta, Phys. Rev. B **77**, 165114 (2008).

[19]L. Zhang, Y. Zhou, L. Guo, W. Zhao, A. Barnes, H. Zhang, C. Eaton, Y. Zheng, M. Brahlek, H. F. Haneef, N. J. Podraza, M. H. W. Chan, V. Gopalan, K. M. Rabe, and R. Engel-Herbert, Nature Materials **15** (2016).

[20]K. Yoshimatsu, K. Okabe, H. Kumigashira, S. Okamoto, S. Aizaki, A. Fujimori, and M. Oshima, Physical Review Letters **104** (2010).

[21]K. Yoshimatsu, K. Horiba, H. Kumigashira, T. Yoshida, A. Fujimori, and M. Oshima, Science **333**, 319 (2011).

[22]G. Koster, B. L. Kropman, G. J. H. M. Rijnders, D. H. A. Blank, and H. Rogalla, Applied Physics Letters **73**, 2920 (1998).

[23]Nist atomic spectra database lines form, https://physics.nist.gov/.

[24]S. Stepanov, E. Kondrashkina, R. Köhler, D. Novikov, G. Materlik, and S. Durbin, Physical Review B **57**, 4829 (1998).